Zitierweise: *Angew. Chem. Int. Ed.* **2023,** *62,* e202301301
Internationale Ausgabe: doi.org/10.1002/anie.202301301
Deutsche Ausgabe: doi.org/10.1002/ange.202301301

Host-Guest Systems | Very Important Paper

π-π Catalysis Made Asymmetric—Enantiomerization Catalysis Mediated by the Chiral π-System of a Perylene Bisimide Cyclophane

Manuel Weh[+], Asja A. Kroeger[+], Kazutaka Shoyama, Matthias Grüne, Amir Karton, and Frank Würthner**

Abstract: Enzymes actuate catalysis through a combination of transition state stabilization and ground state destabilization, inducing enantioselectivity through chiral binding sites. Here, we present a supramolecular model system which employs these basic principles to catalyze the enantiomerization of [5]helicene. Catalysis is hereby mediated not through a network of functional groups but through π-π catalysis exerted from the curved aromatic framework of a chiral perylene bisimide (PBI) cyclophane offering a binding pocket that is intricately complementary with the enantiomerization transition structure. Although transition state stabilization originates simply from dispersion and electrostatic interactions, enantiomerization kinetics are accelerated by a factor of ca. 700 at 295 K. Comparison with the meso-congener of the catalytically active cyclophane shows that upon configurational inversion in only one PBI moiety the catalytic effect is lost, highlighting the importance of precise transition structure recognition in supramolecular enzyme mimics.

Introduction

The catalytic efficiency of biological enzymes is controlled by the intricate interplay between the shapes and characteristics of the active site and the substrates throughout the reaction being catalyzed. The general mode of action of enzyme catalysts can be summarized with reference to comparably simple principles introduced by Pauling[1] and Jencks,[2] according to which reaction barriers are lowered through transition state stabilization originating from shape-complementarity between catalyst and transition structure, and ground state destabilization resulting from non-complementarity between reactant and catalyst.

Perfected by evolution, the catalytic cavities of natural enzymes achieve both exceptional efficiencies and selectivities.[3] From the beginnings of the field, one of the main goals of supramolecular chemistry has been the mimicry of these highly optimized natural catalysts,[4] and strategically designed host–guest systems continue to receive attention as simple artificial mimics of their complex biological counterparts.[5–14] In this context, their well-defined structures, and the possibility of precise control over cavity size and geometry, make cyclophanes promising candidates for synthetic mimics of catalytic cavities.[6,15–21] While many previous explorations of cyclophane catalysis have successfully employed functional groups on the perimeter of the aromatic framework, performing the role of a cofactor,[15–17,22] the inherent presence of aromatic planes makes cyclophanes ideal candidates for studying catalysis by noncovalent π-stacking interactions. Whereas the concepts of cation-π catalysis[21,23] and anion-π catalysis[24,25] are well known, the application of π-π stacking interactions to drive catalysis (π-π catalysis)[26] remains less explored.

In a seminal paper demonstrating this principle, Juríček et al. in 2014 reported the catalysis of the corannulene bowl-inversion by the **ExBox^{4+}** cyclophane.[19] Hereby, experimental and computational analyses revealed that the catalytic effect originates from both, stabilizing π-stacking interactions between the shape-complementary **ExBox^{4+}** host and the planar bowl-inversion transition structure (Figure 1), as well as ground state destabilization due to conformational distortion as a result of non-complementarity between the cavity and the bowl-shaped reagent. Building on this proof-of-concept demonstration of the Pauling–Jencks model, the larger **ExCage^{6+}** host was in 2022 reported to show improved performance as an "artificial racemase" in a study of the inversion catalysis of the less flexible indenocorannulene.[20]

[*] M. Weh,[+] Dr. M. Grüne, Prof. Dr. F. Würthner
Institut für Organische Chemie, Universität Würzburg
Am Hubland, 97074 Würzburg (Germany)
E-mail: wuerthner@uni-wuerzburg.de
Dr. K. Shoyama, Prof. Dr. F. Würthner
Center for Nanosystems Chemistry & Bavarian Polymer Institute, Universität Würzburg
Theodor-Boveri-Weg, 97074 Würzburg (Germany)
Dr. Asja A. Kroeger,[+] Prof. A. Karton
School of Molecular Sciences, The University of Western Australia
35 Stirling Highway, Crawley, WA 6009 (Australia)
E-mail: amir.karton@une.edu.au
Prof. A. Karton
School of Science and Technology, University of New England
Armidale, NSW 2351 (Australia)
[+] These authors contributed equally to this work.

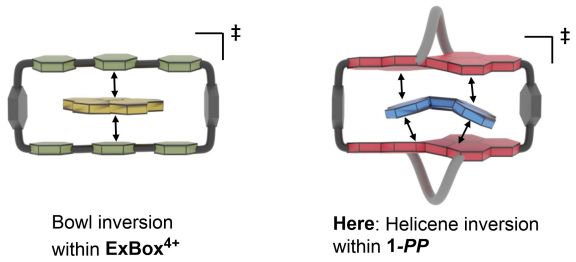

Figure 1. Schematic representation of the transition structure stabilization in the previously reported bowl-to-bowl inversion within the **ExBox**$^{4+}$cyclophane (corannulene's planar transition structure is depicted in yellow, left) and of the enantiomerization of [5]helicene within the chiral PBI cyclophane presented here ([5]helicene's nonplanar transition structure is depicted in blue, right).

Both in nature, as well as in synthesis, catalysis is often aimed towards an enantiomerically enriched product, achieved through the transfer of chiral information from catalyst to substrate.[27–29] In living cells, a complex interplay of kinetics and thermodynamics continuously ensures, with the help of numerous chiral catalysts, that the most entropically stable state, i.e. the racemic mixture, is not reached.[30] The question hence arises, whether it is possible to expand on the above guest-in-box systems such that an asymmetric transformation could be noncovalently catalyzed in the spirit of the Pauling–Jencks model with a cyclophane template.

To this end, following earlier experimental and theoretical work on the binding of planar aromatic hydrocarbons by perylene bisimide (PBI) cyclophanes,[31–35] some of us reported the first inherently chiral PBI cyclophane and discovered the capability of this host to imprint its chiral information onto small carbohelicene guests.[36] Here, we present a complete experimental and computational description of this process via time-dependent CD (circular dichroism) and 2D NMR spectroscopy, single-crystal X-ray crystallography and density functional theory (DFT) calculations. We show that the chiral host not only provides a complementary chiral cavity for binding of the [5]helicene enantiomer of matching helicity, but also provides an ideally shape-matched binding pocket for the enantiomerization transition structure, making this the first example of an artificial "deracemase" capable of effectively catalyzing enantiomerization according to the Pauling–Jencks model of enzyme catalysis purely through the environment of a nonplanar π-system. A comparison with the inactive meso-congener of the active catalyst illustratively demonstrates how, like in natural enzymes,[37] even subtle geometric changes to the binding pocket profoundly affect catalysis. Unlike in previous examples that relied on planarity vs. three dimensionality,[19,20] catalysis originates from the matching of the transition structure's non-planarity with the curvature of the catalyst cavity created by the core twisted PBI moieties (Figure 1), as well as the helicity mismatch between reactant and the host.

Results and Discussion

The distortion of originally planar PBI chromophores into propeller-like twisted structures with *P*- and *M*-helicity by appropriate substitution in the bay positions is a well-established approach.[38–42] While 1,7-di-substitution typically results in conformationally labile derivatives,[39] fast interconversion between the atropo-enantiomers can be prevented via 1,7-bridging units, connecting the two bay positions of the PBI moiety and thus introducing a permanent chiral core twist.[36,38,40] As illustrated in Figure 2, strategic macrocyclization of the resulting chiral PBI chromophores allows for the construction of cyclophanes with an inherently chiral or achiral binding pocket.

As compared to the one-step synthesis recently reported for **1-*PP***,[36] we here employed an improved two-step procedure (Scheme S1) for the synthesis of **1-*PP*** and **1-*MP***, involving imidization of enantiopure perylene bisanhydride (PBA) with the *Boc*-protected *para*-xylylene linker moieties and subsequent macrocyclization with the corresponding second PBA of desired configuration (for the full synthetic procedure, see the Supporting Information). X-ray crystallographic analysis of a single crystal of the newly synthesized **1-*MP*** confirms its structure and reveals a mirror plane perpendicular to the *para*-xylylene spacer units (Figure S23).[43] In contrast to **1-*PP***, where the facing

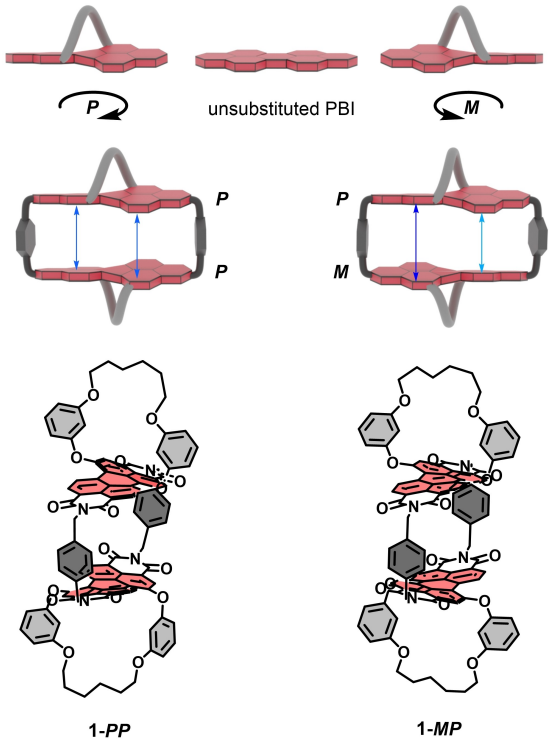

Figure 2. Schematic depictions of the concept of inducing *P*- and *M*-helicity in PBIs as well as the geometrical differences between the two cyclophane isomers **1-*PP*** and **1-*MP*** and their molecular structures. The blue double arrows indicate the non-parallel orientation of the naphthalene units in the case of the meso host, resulting in a varying cavity height, and the parallel face-to-face orientation between them in the homochiral congener.

naphthalene units of the PBI chromophores are arranged in a parallel manner, the naphthalene units in the dye moieties of **1-*MP*** have a non-parallel orientation, resulting in an achiral cavity with varying height (≈6.5–8.1 Å).

Fluorescence titration studies (Figure S7) were employed to provide insights into the effect of the structural difference between the two hosts on the binding strength for the [5]helicene guest. Whereas complexation of *P*-[5]helicene by **1-*PP*** results in a high association constant of $K_a = 1.6 \times 10^9\ M^{-1}$ in tetrachloromethane,[36] a reduced association constant of $K_a = 2.0 \times 10^6\ M^{-1}$ is observed in the same solvent for the complexation of *rac*-[5]helicene by the meso cyclophane. Accordingly, while the inversion of configuration in one chromophoric unit of **1-*MP*** disturbs the shape match between host and guest, a shape complementarity between **1-*PP*** and [5]helicene of the same configuration allows for very efficient complexation.

In order to investigate the influence of the chiral environment on [5]helicene within **1-*PP***, we carried out proton NMR experiments to shine light on the complex structure. Taking into account the enantiomerization barrier of around 100 kJ mol^{-1} for [5]helicene,[44] we prepared an equilibrated 1:1 mixture of racemic guest and **1-*PP*** in 1,1,2,2-tetrachloroethane-d_2, which indeed revealed sharp and well resolved signals at a temperature of 245 K (Figure 3a). The protons of the host split into two sets of signals with equal integrals in the slow exchange regime owing to a desymmetrization of the free host (point group D_2 on the NMR time scale) upon the binding of [5]helicene (point group C_2). The guest protons give one signal set whose integrals fit the expected 1:1 complex. Notably, the addi-

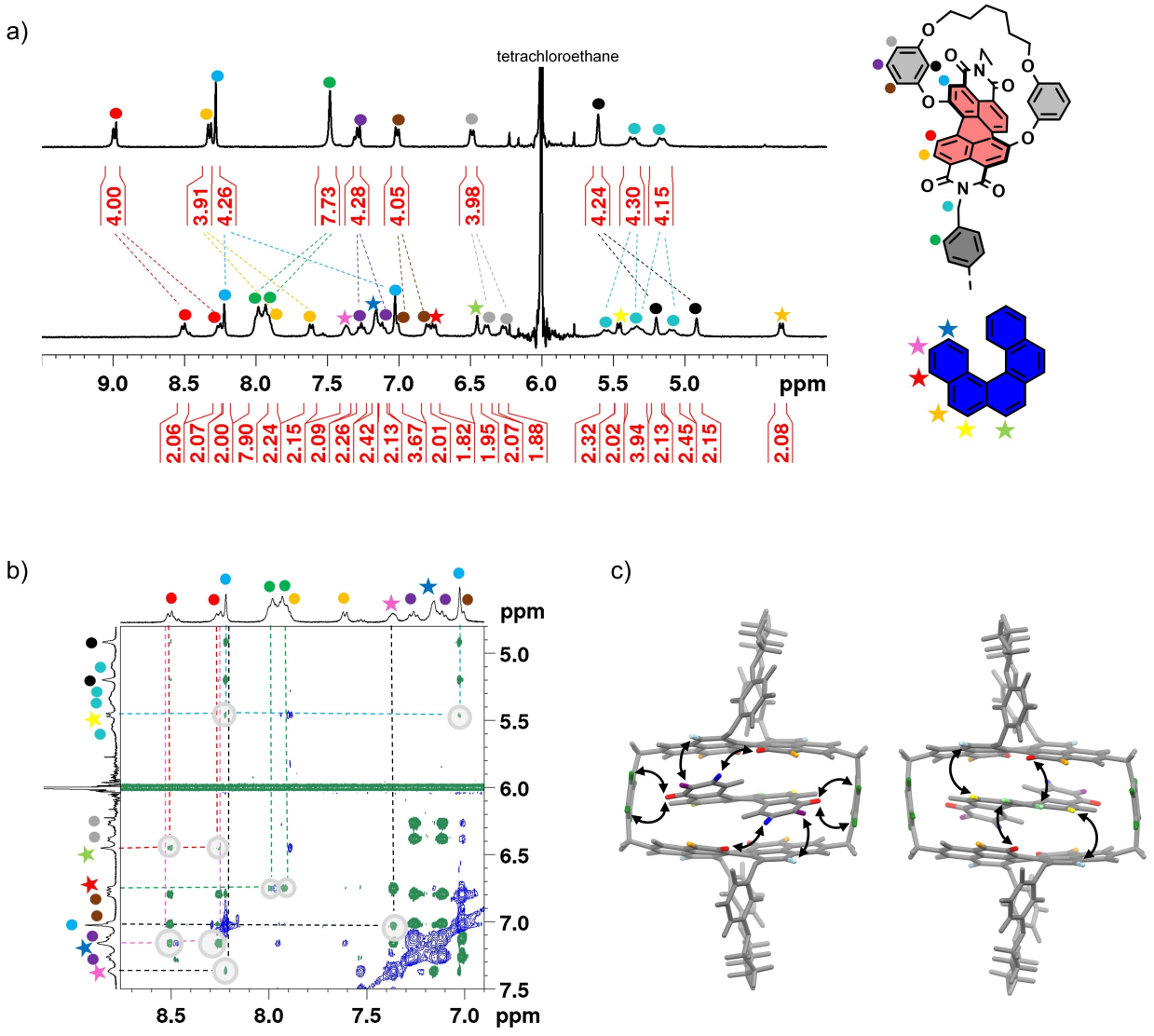

Figure 3. a) Low-temperature NMR (245 K, 400 MHz) spectrum of **1-*PP*** in the absence and in the presence of one equivalent of *rac*-[5]helicene in tce-d_2 (c (**1-*PP***) ≈ 1.0 mM). The guest proton in the 1-position could not be resolved. b) Excerpt from the ^{1}H-^{1}H ROESY NMR (600 MHz) of **1-*PP*** (c ≈ 1.0 mM) and *rac*-[5]helicene (one equivalent) in tce-d_2 at 245 K. The relevant cross-signals are highlighted in grey. c) Geometry optimized structure of *P*-[5]helicene⊂**1-*PP*** viewed from the two sides with double arrows highlighting the cross-signals between host and guest protons.

tional set of signals for the host protons can not be explained by a splitting due to partial complexation, which was confirmed by a comparison of the spectra in the absence and the presence of the guest molecule, showing that none of the signals in the spectrum correspond to the free host protons. Furthermore, our computational studies (see below) on the epimeric complexes, i.e. *P*-[5]helicene⊂**1-*PP*** and *M*-[5]helicene⊂**1-*PP***, give strongly different complexation energies, which is in accordance with our observation that only one complex species, i.e. *P*-[5]helicene⊂**1-*PP***, is present in solution. All proton signals of the complex could be assigned with the help of 2D NMR spectroscopy at low temperature (Figure S15 and S16). In order to elucidate the binding mode, a ^{1}H-^{1}H ROESY NMR (Figure 3b and S16) experiment was carried out. Distinct cross-signals were observed not only between the chromophore and the guest unit but also between the aromatic spacer protons of the cyclophane and the guest protons, revealing spatial proximity between the corresponding subunits. These correlations support a perfectly embedded guest within the receptor's cavity (Figure 3c). Surprisingly, cross-signals of identical intensity between the corresponding guest proton and both signal sets of the host can be observed in the ROESY spectrum, indicating a reversible conformational change, proceeding with a similar barrier in both directions. We note that the cross-signals indicate a dynamic rotation of the guest within the cavity, which we find from variable temperature NMR and ^{1}H-^{1}H EXSY NMR to proceed with a barrier of around 54 kJ mol^{-1}. For details on this dynamic motion, we refer to the Supporting Information.

In order to further examine the conclusion drawn from NMR studies, we grew a co-crystal from a mixture of **1-*PP*** and racemic [5]helicene, suitable for single-crystal X-ray analysis, by slow diffusion of *n*-hexane into a chlorobenzene solution of the mixture (Figure 4).[43] The molecules in this crystal pack in the monoclinic system with no contact between the π-surfaces of the PBI units of neighboring cyclophanes. The space between the chromophores of the adjacent cyclophane PBI units is filled with solvent molecules (Figure S24), which were partially removed by the SQUEEZE routine in our crystallographic analysis.[45] The X-ray structure unambiguously confirms the formation of a 1:1 complex as suggested by the NMR studies. More importantly, in line with our expectations based on NMR spectroscopy and theory, the guest exists only in its *P*-configuration within the cavity of the **1-*PP*** host, which supports the conclusion that the homochiral complex is the thermodynamically favored state. The shape match between the helical structure of the guest and the PBI chromophores gives rise to a right-handed supramolecular helix with three turns. For the PBI chromophores, the angle between the naphthalene units (the core twist) is with 21.2° increased by 6° compared to a crystal structure with [4]helicene[36] in order to accomodate the higher steric demand of the guest.

Notably, the solid-state structure further reveals that the dihedral angle spanned by the planes of the outer naphthalene units of [5]helicene, is significantly compressed. While a dihedral angle of 30.4° was found for [5]helicene in the complex with the PBI cyclophane, this angle is, at 41.4°, significantly larger in the crystal structure of the free guest reported in literature.[46] Both values, as well as observed PBI core twists are in good agreement with those obtained from theoretical calculations (see below).

Our NMR and single-crystal X-ray analyses suggest the formation of one single complex structure from a mixture of racemic [5]helicene and **1-*PP***. Thus, in order to investigate the interaction between [5]helicene and **1-*PP*** further, we carried out detailed studies on the enantiomerization process of the guest. The kinetics of the chirality inversion of [5]helicene were studied in the absence and in the presence of 2 equiv of **1-*PP*** and **1-*MP*** using time-dependent CD spectroscopy. Figure 5a shows the CD time course of *M*-[5]helicene in the absence and in the presence of **1-*MP***, while Figure 5b displays the time-dependent CD changes of both *P*- and *M*-[5]helicene in the presence of **1-*PP***. We note that repetition of the CD studies using larger excesses of host (5 equiv and 10 equiv) had almost no influence on the enantiomerization kinetics (Figure S13), confirming guest enantiomerization rather than complexation or decomplexation to be rate-determining and therefore allowing quantitative conclusions on the guest isomerization from the optical changes.

As apparent from Figure 5 and Figures S8–S12, in all three cases, the curves of the time courses could be properly fitted according to first-order kinetics [Eq. (S1)]. The resulting first-order kinetics fits allow calculation of racemization and enantiomerization rate constants. Hereby it is instructive to note that the changing CD signals over the two time courses represented in Figure 5a, namely the time courses for *M*-[5]helicene in the absence of a host (black symbols) and in the presence of **1-*MP*** (grey symbols), indicate racemization of the sample within approximately 35 h.

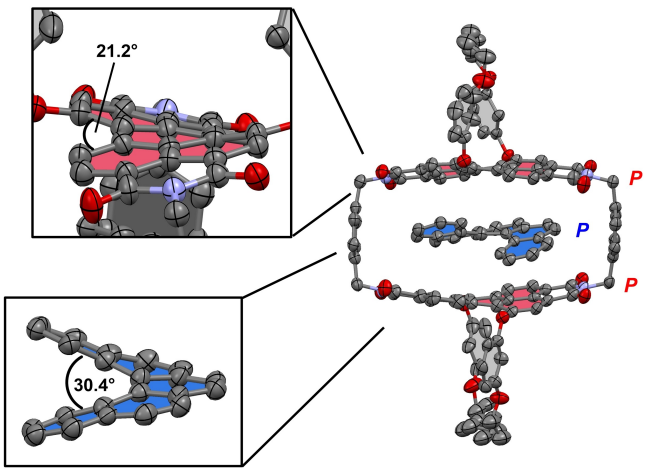

Figure 4. Molecular structure of the *P*-[5]helicene⊂**1-*PP*** complex from single-crystal X-ray analysis (thermal ellipsoids set at 50% probability). The guest is highlighted in blue, the perylene units are highlighted in red. Zoom-ins of one chromophore unit as well as of the guest are given to visualize the mutual adaption of host and guest in this system. Solvent molecules and hydrogen atoms are omitted for clarity.

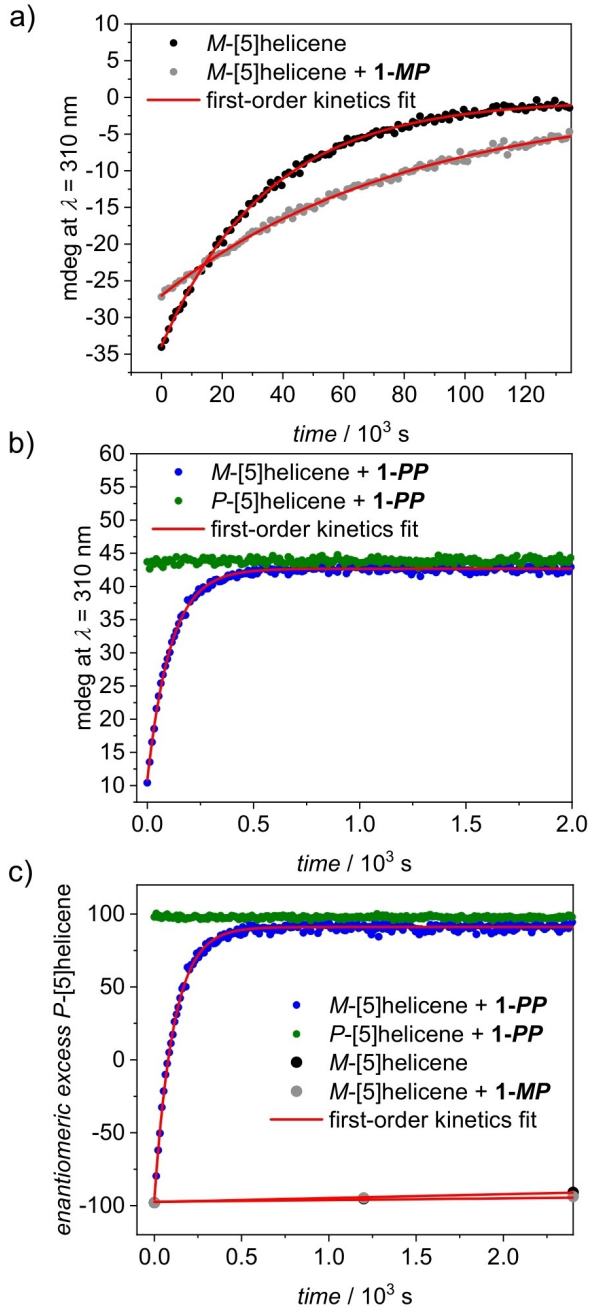

Figure 5. a) Time course of the CD signal of *M*-[5]helicene ($c = 10\ \mu M$) at 22 °C in the presence and in the absence of **1-*MP*** ($c = 20\ \mu M$, 2 equiv) and the fitting curves according to first-order kinetics. b) Time course of the CD signal of *M*-[5]helicene and *P*-[5]helicene ($c = 10\ \mu M$) at 22 °C in the presence of **1-*PP*** ($c = 20\ \mu M$, 2 equiv). c) The corresponding time courses of the enantiomeric excess of *P*-[5]helicene (−100% corresponds to enantiopure *M*-[5]helicene), calculated according to $ee = \Delta\varepsilon/\Delta\varepsilon_{max}$.[50]

In contrast, the comparison between the time courses of *P*-[5]helicene and *M*-[5]helicene in the presence of **1-*PP*** suggests formation of a stable homochiral complex in both cases. Confirming helical self-recognition, the CD signal remains unchanged throughout the time course for *P*-[5]helicene in the presence of **1-*PP*** (Figure 5b, green symbols). The equilibrated state reached for the mixture of **1-*PP*** and *M*-[5]helicene (Figure 5b, blue symbols) gives the same CD signal as the homochiral host–guest mixture, indicating formation of the same homochiral complex and almost full conversion of *M*-[5]helicene into *P*-[5]helicene. Accordingly, the fits given in Figure 5a give rate constants, where $k_{obs} = k_{rac}$, from which enantiomerization rate constants can be obtained as $k_{rac} = 2k_e$.[47,48] From the fit corresponding to the CD time course of *M*-[5]helicene in the presence of **1-*PP*** in the typical absorption range of the substrate, the enantiomerization rate constant can be obtained as $k_{obs} = k_e$.

For the enantiomerization of [5]helicene at room temperature in the absence of a host, we determined a rate constant of $k_{e,uncat} = 1.4 \times 10^{-5}\ s^{-1}$, corresponding to a Gibbs free enantiomerization barrier of $99.6\ kJ\,mol^{-1}$ [Eq. (S2)]. This is in good agreement with previous literature.[44,49] In the presence of an excess of **1-*MP***, it is apparent from the time course that the racemization process is weakly decelerated, indicating a small inhibitive effect of the meso cyclophane on the guest enantiomerization. Confirming this observation, we indeed obtain a reduced enantiomerization rate constant of $k_{e,\mathbf{1\text{-}MP}} = 6.1 \times 10^{-6}\ s^{-1}$, corresponding to a slightly increased Gibbs free enantiomerization barrier of $101.7\ kJ\,mol^{-1}$.

In contrast, in the presence of the homochiral cyclophane **1-*PP***, the observed CD changes suggest a significant acceleration of the enantiomerization of *M*-[5]helicene. While the uncatalyzed racemization of [5]helicene occurred on a timescale of more than a day, we find that in the presence of **1-*PP*** the enantioenriched equilibrium is reached within several minutes. Accordingly, we obtain a notably increased enantiomerization rate constant of $k_{e,\mathbf{1\text{-}PP}} = 9.1 \times 10^{-3}\ s^{-1}$, corresponding to a significantly lowered barrier of $83.7\ kJ\,mol^{-1}$ at room temperature. This enantiomerization barrier was further validated by an Eyring analysis (Figure S14) using temperature-dependent CD studies (Figure S8, S9, S11 and S12). For the full results, including enthalpic and entropic contributions, see the Supporting Information (Table S1). In order to illustrate the difference between the kinetics, a combined plot of Figure 5a,b is depicted in Figure 5c, which shows the time-dependent enantiomeric excess of all described processes. From this depiction, the dramatic acceleration of the guest enantiomerization in the presence of **1-*PP*** becomes apparent. The ratio of the enantiomerization rate constants in the presence and the absence of **1-*PP*** reveals a ≈700-fold acceleration of the uncatalyzed enantiomerization process, and a catalytic rate enhancement of $k_{e,\ \mathbf{1\text{-}PP}}/k_{e,\ \mathbf{1\text{-}MP}} \approx 1600$ compared to the enantiomerization within the achiral host. Thus, we find not only a notable catalytic effect of **1-*PP*** on the [5]helicene enantiomerization, but also a significant effect of an apparently small change in cavity geometry on catalytic efficiency.

In order to identify the origin of this catalytic effect, as well as the observed difference in catalytic activity of **1-*PP*** and **1-*MP***, we carried out computational studies to gain insights into the structural features of the complexes and noncovalent interactions along the reaction coordinates of

the inversion of [5]helicene in the presence and absence of the hosts. We begin by considering the uncatalyzed enantiomerization process of [5]helicene. Figure 6 shows the resulting equilibrium and transition structure (TS) geometries optimized at the B3LYP-D3(BJ)/def2-SVP level of theory[51–57] along with the associated enantiomerization barrier obtained at the SMD-(CCl_4)-PW6B95-D3(BJ)/def2-TZVPP level of theory.[55–59]

Unlike the processes studied in previous research on cyclophane catalyzed isomerizations,[19,20,34,35] the chirality inversion of [5]helicene proceeds via a distinctly nonplanar TS with a puckered, C_s symmetric geometry. The associated Gibbs free energy barrier for this process of 102.2 kJ mol^{-1} obtained here is in good agreement with experimental data (see above), as well as high-level ab initio calculations.[60] To subsequently determine how this process is affected by complexation with the present hosts, we optimized all reactant, transition structure, and product complexes with **1-*PP*** and **1-*MP*** and performed energy decomposition analyses (EDAs) using the second generation of the absolutely localized molecular orbital (ALMO) EDA scheme by Head-Gordon and co-workers[61] on the resulting complexes. Figure 7 gives schematic potential energy profiles for the chirality inversion of [5]helicene in the presence of **1-*PP*** and **1-*MP***, as well as breakdowns of the relative noncovalent TS stabilizations and destabilizations from EDAs (for full EDA results for all complexes, see Table S5). Table 1 provides a summary of the kinetic and thermodynamic parameters of these processes obtained experimentally and computationally.

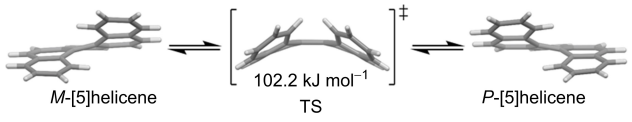

Figure 6. Optimized equilibrium and transition structures pertaining to the enantiomerization of [5]helicene along with the corresponding Gibbs free enantiomerization barrier at 298 K.

In agreement with experimental observations, for the enantiomerization occurring within the cavity of **1-*PP***, we obtain a reduced barrier of 93.7 kJ mol^{-1}, whereas a calculated barrier of 102.8 kJ mol^{-1} in the presence of **1-*MP*** confirms the observed catalytic inactivity of this host. Confirming the observation of deracemization by **1-*PP*** from preceding experimental studies (see above), we further find a notable relative stabilization of 15.3 kJ mol^{-1} of *P*-[5]helicene over *M*-[5]helicene, which becomes apparent upon visual inspection of the optimized host–guest complexes. In *P*-[5]helicene⊂**1-*PP***, the matching handedness of

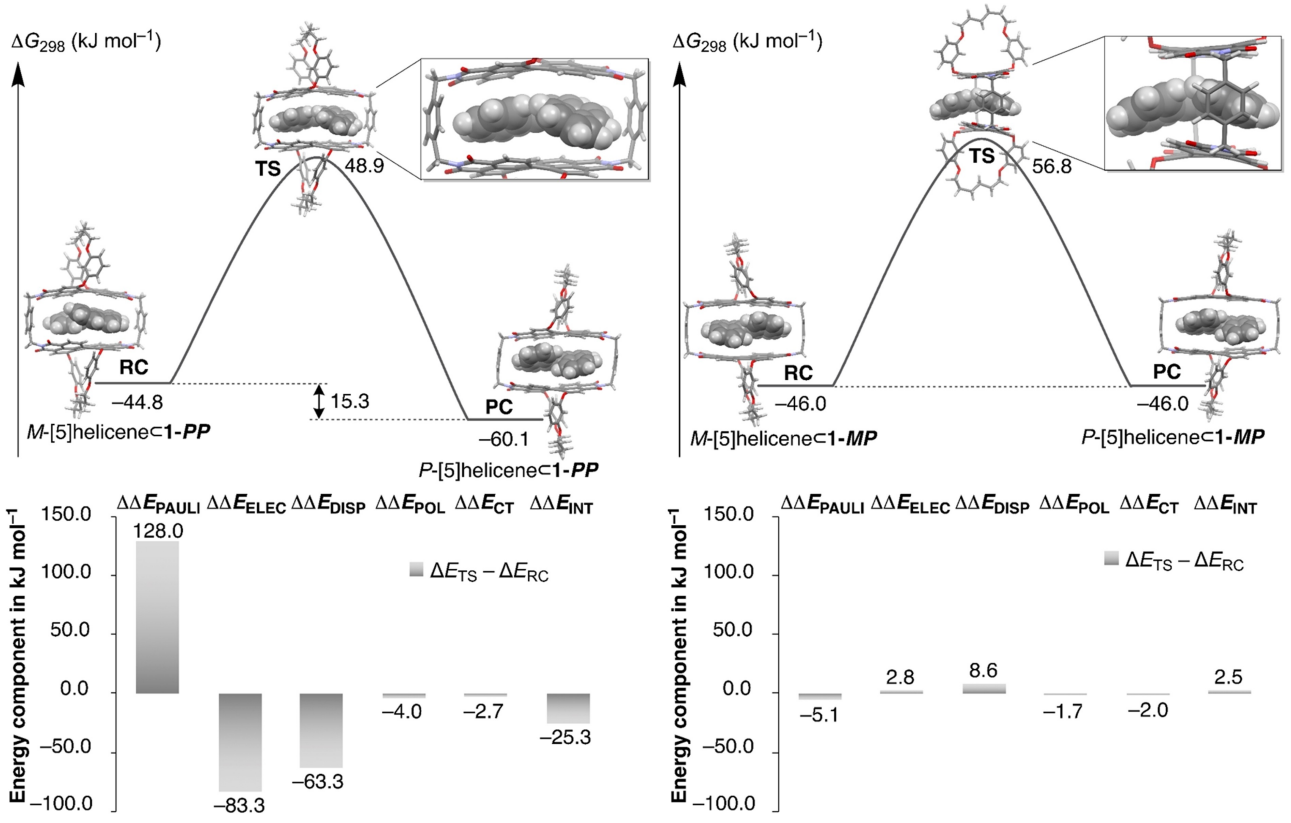

Figure 7. Schematic PESs of the [5]helicene inversions within **1-*PP*** and **1-*MP*** (Gibbs free energies at 298 K are given in kJ mol^{-1} relative to the free reactants) along with breakdowns of relative noncovalent stabilizations and destabilizations of TSs obtained from EDAs, calculated as $\Delta\Delta E = \Delta E_{TS} - \Delta E_{RC}$. (RC = reactant complex, PC = product complex; geometries and energies were obtained at the SMD-(CCl_4)-PW6B95-D3(BJ)/def2-TZVPP//B3LYP-D3(BJ)/def2-SVP level of theory,[55–59] while ALMO-EDA[61] analyses were performed using the ωB97M-V/def2-SVP level of theory).[57,62]

Table 1: Summary of the most important thermodynamic and kinetic data of [5]helicene in the presence of **1-*PP*** and **1-*MP***..

	K_a [M^{-1}][a)]	$\Delta G_{exp.}$[b] ($\Delta G_{comp.}$) [kJ mol^{-1}]	k_e [s^{-1}]	$k_e/k_{e,uncat}$	$\Delta G^{\ddagger}_{exp.}$ ($\Delta G^{\ddagger}_{comp.}$)[c] [kJ mol^{-1}]	$\Delta\Delta G^{\ddagger}_{exp.}$ ($\Delta\Delta G^{\ddagger}_{comp.}$)[d] [kJ mol^{-1}]
1-*PP*	1.6×10^{9}	−52.0 (−60.1)	9.1×10^{-3}	6.5×10^{2} [e]	83.7 (93.7)	15.9 (8.5)
1-*MP*	2.0×10^{6}	−35.6 (−46.0)	6.1×10^{-6}	4.4×10^{-1}	101.7 (102.8)	−2.1 (−0.6)

[a] Obtained from complexation studies of *P*-[5]helicene with **1-*PP***[36] and *rac*-[5]helicene with **1-*MP***. [b] Calculated from $\Delta G_{exp.} = -RT\ln K_a$, with R being the ideal gas constant and the respective binding constant K_a at 295 K. [c] Calculated from the Eyring equation with $\Delta G^{\ddagger}_{exp.} = -RT\ln(k_e h/k_b T)$ with the ideal gas constant R, the Planck constant h and the Boltzmann constant k_b at 295 K. [d] Calculated from $\Delta\Delta G^{\ddagger}_{exp.} = \Delta G^{\ddagger}_{non.} - \Delta G^{\ddagger}_{exp.}$, where $\Delta G^{\ddagger}_{non.}$ corresponds to the experimentally determined enantiomerization barrier of [5]helicene of 99.6 kJ mol^{-1}. [e] With 5 or 10 equiv, the ratio is slightly increased to $k_e/k_{e,uncat} = 7.9\times10^{2}$.

the guest's and the host's π-systems allows for the complex to arrange into a highly stabilized π-stack resembling a helix with three turns. In contrast, the chirality mismatch between the guest and the hosts' PBI moieties in *M*-[5]helicene⊂**1-*PP*** and both [5]helicene⊂**1-*MP*** complexes leads to non-ideal host–guest complementarity and smaller stabilization energies, which are similar for both types of complexes. As this shows that the observed striking difference in catalytic activities of **1-*PP*** and **1-*MP*** is not due to differential stabilization of reactant complexes, the origin of relative stabilization of the achiral puckered enantiomerization TS by **1-*PP*** is less apparent.

Inspection of the optimized TS complex with **1-*PP*** reveals that the parallel orientation of the host's naphthalene moieties creates a consistent cavity height, while the core twist of the PBI moieties creates curvature in the π-systems. This curvature intricately matches the curvature of the puckered TS, allowing for the nonplanar π-system of the TS to be noncovalently stabilized in the binding pocket by π-stacking with the nonplanar π-system of the host. In contrast, the variation in cavity height created by the non-parallel naphthalene units of **1-*MP*** and the opposing orientations of the PBI core twists create non-complementary nonplanarity in the host's and the TS's π-systems and reduce noncovalent TS stabilization by **1-*MP***.

Results from energy decomposition analyses provide a breakdown of the overall intermolecular interactions between host and guest structures, allowing us to quantify these qualitative observations. As apparent from Figure 7, in the TS complex with **1-*MP***, relative TS stabilizations and destabilizations are consistently minute, leading to no overall relative noncovalent stabilization of the TS by **1-*MP***. In contrast, a very different picture emerges for the enantiomerization process within **1-*PP***. Here, the comparably larger Pauli repulsions in the TS complex compared to *M*-[5]helicene⊂**1-*PP*** confirm a more closely interacting TS complex. Outweighing this destabilizing contribution, electrostatic and dispersion interactions, characteristic of π-stacked complexes,[63,64] emerge as the largest source of absolute (Table S5) as well as relative TS stabilization. Notably, these contributions are not just larger in the TS complex than in the *M*-[5]helicene⊂**1-*PP*** reactant complex, but also by 35.2 kJ mol^{-1} (ΔE_{ELEC}) and 20.0 kJ mol^{-1} (ΔE_{DISP}) larger in the TS complex than the homochiral *P*-[5]helicene⊂**1-*PP*** product complex (Table S5). This indicates that π-π stacking interactions are indeed maximized in the complex between the intricately complementary transition structure and **1-*PP***, even when compared to the homochiral *P*-[5]helicene⊂**1-*PP*** complex, thereby corroborating a significant contribution of TS stabilization to the catalytic effect.

Aside from TS stabilization, destabilization of the reactant complex due to geometric distortions in host and guest resulting from the binding of the less complementary reactant is expected to contribute to overall reaction barrier lowering according to the Pauling–Jencks model of enzyme catalysis.[1,2] In order to quantify this ground state destabilization in our systems of interest, we calculate the differences in electronic energies (ΔE_e) between free equilibrium host and guest structures and the corresponding geometries of the isolated host and guest molecules, respectively, in reactant, transition structure, and product complexes. Figure 8a,b gives the destabilization energies resulting for the host and guest moieties of all complexes.

As clearly apparent from Figure 8a, for the process catalyzed by **1-*PP***, destabilization energies decrease along the reaction coordinate. While host and guest in the "helicity-mismatched" reactant complex receive the largest overall destabilization of 16.8 kJ mol^{-1}, the total destabilizations of the more complementary host and guest of the TS and homochiral product complexes amount to only 11.7 and 7.8 kJ mol^{-1}, respectively. Thus, in accordance with the Pauling–Jencks model, a comparably smaller destabilization of host and guest in the TS complex compared to the reactant complex (by 5.1 kJ mol^{-1}, overall) contributes to the overall catalytic effect observed for this system. By comparison, for the process occurring within the less complementary host **1-*MP***, Figure 8b shows that the reactant and transition structure complexes are destabilized to almost the same extent (by overall 16.2 and 15.7 kJ mol^{-1}, respectively), indicating a negligible effect of ground state destabilization on the enantiomerization barrier. In agreement with the well-documented flexibility of the bay regions of PBIs,[65,66] we note that the calculated destabilizations of the guest are consistently larger than those of the host and originate from the guest planarizing in response to the geometric constraints of the hosts' cavities.

Figure 8c summarizes the results of the computational investigation into the origins of the catalytic effect of the chiral host **1-*PP*** on the [5]helicene enantiomerization. As apparent from the schematic illustrations, the observed reaction barrier lowering originates both from transition state stabilization, as well as ground state destabilization, in line with the Pauling–Jencks model. Hereby, EDAs (Fig-

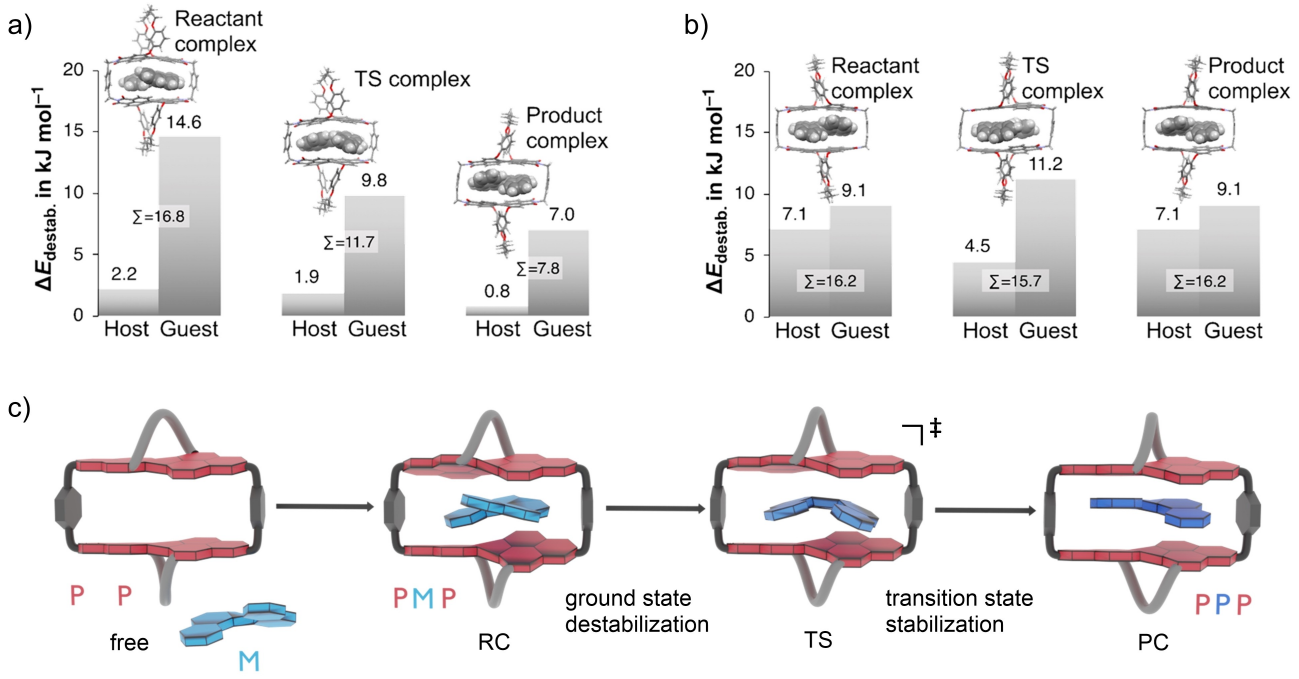

Figure 8. Differences in electronic energies ($\Delta E_{destab.}$) between corresponding host and guest structures from free optimizations and from optimizations of reactant, transition structure (TS), and product complexes for the enantiomerization process within a) **1-*PP*** and b) **1-*MP*** in kJ mol^{-1}. c) Schematic representation of the whole enantiomerization process of [5]helicene within **1-*PP***.

ure 7) showed that TS stabilization is almost exclusively the result of stabilizing electrostatic and dispersion interactions resulting from optimized π-π stacking interactions between the neatly aligned curved π-systems of the enantiomerization TS and the host. While the catalytic cavities of natural enzymes typically rely on complex networks of functional groups, the present system represents an attractively simple example of a catalytic process in which TS stabilization is achieved purely through π-π stacking. Compared to the first examples of such "π-π catalysis", which explored proof-of-principle inversion processes with isoenergetic reactants and products,[19,20,26,34,35] the inherent chirality of the present PBI cyclophane host for the first time introduces a non-zero reaction energy and thus achieves π-π catalysis with significant enantioselectivity despite its simplicity. Contributing to the catalytic effect resulting from TS stabilization, ground state destabilization results from a shape mismatch between the *M*-[5]helicene reactant and the *P*-homochiral host, necessitating energetically unfavorable geometric distortions in the reactant complex. This "strain energy" is released in the more geometrically relaxed TS complex. In contrast, the shape-mismatch between the enantiomerization TS and the cavity of **1-*MP*** leads to the loss of relative noncovalent TS stabilization, and destabilizing geometric distortions in the TS complex largely outweigh the contribution from ground state destabilization. Thus, the computational model comprehensively explains both, the origins of the catalytic effect of the "active deracemase" **1-*PP***, as well as the origins of the loss of catalytic activity upon the comparably small geometric modification to the host's cavity that results from chirality inversion in one PBI moiety.

Conclusion

In summary, we have reported a detailed experimental and computational study for a helicene enantiomerization process that is promoted in an enzyme-like manner by the cavity of an inherently chiral PBI cyclophane. We find that the curvature of the host's π-system not only exhibits favored recognition of the helicene enantiomer of matching handedness, but furthermore an intricate match in cavity shape and π-system curvature between the host's PBI moieties and the nonplanar [5]helicene enantiomerization transition structure also makes the cyclophane a complementary receptor for the transition structure. By comparison, the complex with the helicity mismatched [5]helicene enantiomer receives reduced noncovalent stabilization and experiences more significant destabilizing geometric distortions. In this fashion, the here described host actuates noncovalent catalysis according to the Pauling–Jencks model of enzyme catalysis by stabilizing the transition structure and destabilizing the ground state. EDA analyses show that transition structure stabilization primarily originates from noncovalent dispersion and electrostatic interactions between the nonplanar π-systems of the [5]helicene guest and the host. Time-dependent CD studies find the enantiomerization barrier to be significantly reduced, allowing for rapid formation (ca. 700 times rate acceleration) of the homochiral complex, which is confirmed by 2D NMR spectroscopy and crystallographic studies. A comparison with the meso-congener of the catalytically active chiral cyclophane shows that changing the handedness of only one PBI moiety not only affects chiral recognition, but also transforms the host from an

effective catalyst into a slight inhibitor of enantiomerization. Thus, this study not only provides a detailed description of deracemization catalysis actuated by a chiral host, but also highlights the importance of precise transition structure recognition in the development of supramolecular enzyme mimics.

Acknowledgements

We thank the Fonds der Chemischen Industrie for a Kekulé fellowship for M.W. We further gratefully acknowledge the provision of a Forrest Research Foundation Scholarship and an Australian Government Research Training Program Stipend (to A.A.K.) and an Australian Research Council (ARC) Future Fellowship (to A.K.; project no. FT170100373). We gratefully acknowledge generous allocations of computing time from the National Computational Infrastructure (NCI), supported by the Australian Government, as well as system administration support provided by the Faculty of Science at the University of Western Australia to the Linux cluster of the Karton group. We acknowledge DESY (Hamburg, Germany), a member of the Helmholtz Association HGF, for providing experimental facilities at PETRA III (proposal No STP-20211168) for solving the complex structure by single-crystal X-ray analysis. We thank Dr. Eva Crosas for assistance in using P11. Open Access funding enabled and organized by Projekt DEAL.

Conflict of Interest

The authors declare no conflict of interest.

Data Availability Statement

The data that support the findings of this study are available from the corresponding author upon reasonable request.

Keywords: Cyclophane · Enantiomerization · Helicene · Perylene Bisimide · Supramolecular π-π Catalysis

[1] L. Pauling, *Nature* **1948**, *161*, 707–709.
[2] W. P. Jencks, *Catalysis in chemistry and enzymology*, Courier Corporation, Chelmsford, **1987**.
[3] R. Wolfenden, M. J. Snider, *Acc. Chem. Res.* **2001**, *34*, 938–945.
[4] D. J. Cram, *Angew. Chem. Int. Ed. Engl.* **1988**, *27*, 1009–1020.
[5] T. Habicher, F. Diederich, V. Gramlich, *Helv. Chim. Acta* **1999**, *82*, 1066–1095.
[6] F. Diederich, *Angew. Chem. Int. Ed. Engl.* **1988**, *27*, 362–386.
[7] C. Kremer, A. Lützen, *Chem. Eur. J.* **2013**, *19*, 6162–6196.
[8] H. Zhou, X.-Y. Pang, X. Wang, H. Yao, L.-P. Yang, W. Jiang, *Angew. Chem. Int. Ed.* **2021**, *60*, 25981–25987.
[9] X. Huang, X. Wang, M. Quan, H. Yao, H. Ke, W. Jiang, *Angew. Chem. Int. Ed.* **2021**, *60*, 1929–1935.
[10] J. Kang, J. Rebek, *Nature* **1997**, *385*, 50–52.
[11] M. Yoshizawa, M. Tamura, M. Fujita, *Science* **2006**, *312*, 251–254.
[12] Y. Lyu, P. Scrimin, *ACS Catal.* **2021**, *11*, 11501–11509.
[13] A. J. Kirby, *Angew. Chem. Int. Ed. Engl.* **1996**, *35*, 706–724.
[14] M. Morimoto, S. M. Bierschenk, K. T. Xia, R. G. Bergman, K. N. Raymond, F. D. Toste, *Nat. Catal.* **2020**, *3*, 969–984.
[15] H.-D. Lutter, F. Diederich, *Angew. Chem. Int. Ed. Engl.* **1986**, *25*, 1125–1127.
[16] F. Diederich, H. D. Lutter, *J. Am. Chem. Soc.* **1989**, *111*, 8438–8446.
[17] A. J. Kennan, H. W. Whitlock, *J. Am. Chem. Soc.* **1996**, *118*, 3027–3028.
[18] M. Raynal, P. Ballester, A. Vidal-Ferran, P. W. N. M. van Leeuwen, *Chem. Soc. Rev.* **2014**, *43*, 1734–1787.
[19] M. Juríček, N. L. Strutt, J. C. Barnes, A. M. Butterfield, E. J. Dale, K. K. Baldridge, J. F. Stoddart, J. S. Siegel, *Nat. Chem.* **2014**, *6*, 222–228.
[20] Y. Wang, M. Rickhaus, O. Blacque, K. K. Baldridge, M. Juríček, J. S. Siegel, *J. Am. Chem. Soc.* **2022**, *144*, 2679–2684.
[21] D. A. Stauffer, R. E. Barrans Jr, D. A. Dougherty, *Angew. Chem. Int. Ed. Engl.* **1990**, *29*, 915–918.
[22] Y. Murakami, J.-i. Kikuchi, Y. Hisaeda, O. Hayashida, *Chem. Rev.* **1996**, *96*, 721–758.
[23] A. McCurdy, L. Jimenez, D. A. Stauffer, D. A. Dougherty, *J. Am. Chem. Soc.* **1992**, *114*, 10314–10321.
[24] Y. Zhao, C. Beuchat, Y. Domoto, J. Gajewy, A. Wilson, J. Mareda, N. Sakai, S. Matile, *J. Am. Chem. Soc.* **2014**, *136*, 2101–2111.
[25] Y. Zhao, Y. Cotelle, L. Liu, J. López-Andarias, A.-B. Bornhof, M. Akamatsu, N. Sakai, S. Matile, *Acc. Chem. Res.* **2018**, *51*, 2255–2263.
[26] A. A. Kroeger, A. Karton, *Chem. Eur. J.* **2021**, *27*, 3420–3426.
[27] C. Tan, D. Chu, X. Tang, Y. Liu, W. Xuan, Y. Cui, *Chem. Eur. J.* **2019**, *25*, 662–672.
[28] C. García-Simón, R. Gramage-Doria, S. Raoufmoghaddam, T. Parella, M. Costas, X. Ribas, J. N. H. Reek, *J. Am. Chem. Soc.* **2015**, *137*, 2680–2687.
[29] C. Zhao, Q.-F. Sun, W. M. Hart-Cooper, A. G. DiPasquale, F. D. Toste, R. G. Bergman, K. N. Raymond, *J. Am. Chem. Soc.* **2013**, *135*, 18802–18805.
[30] *Comprehensive Supramolecular Chemistry, Vol. 4* (Eds.: J. L. Atwood, J. E. D. Davies, D. D. MacNicol, F. Vögtle, Y. Murakami), Elsevier Science, Oxford, **1996**.
[31] P. Spenst, F. Würthner, *Angew. Chem. Int. Ed.* **2015**, *54*, 10165–10168.
[32] P. Spenst, A. Sieblist, F. Würthner, *Chem. Eur. J.* **2017**, *23*, 1667–1675.
[33] M. Sapotta, A. Hofmann, D. Bialas, F. Würthner, *Angew. Chem. Int. Ed.* **2019**, *58*, 3516–3520.
[34] A. A. Kroeger, A. Karton, *Org. Chem. Front.* **2021**, *8*, 4408–4418.
[35] A. A. Kroeger, A. Karton, *J. Org. Chem.* **2022**, *87*, 5485–5496.
[36] M. Weh, J. Rühe, B. Herbert, A.-M. Krause, F. Würthner, *Angew. Chem. Int. Ed.* **2021**, *60*, 15323–15327.
[37] D. E. Koshland, Jr., *Angew. Chem. Int. Ed.* **1995**, *33*, 2375–2378.
[38] P. Osswald, M. Reichert, G. Bringmann, F. Würthner, *J. Org. Chem.* **2007**, *72*, 3403–3411.
[39] P. Osswald, F. Würthner, *J. Am. Chem. Soc.* **2007**, *129*, 14319–14326.
[40] M. M. Safont-Sempere, P. Osswald, K. Radacki, F. Würthner, *Chem. Eur. J.* **2010**, *16*, 7380–7384.
[41] R. Renner, B. Mahlmeister, O. Anhalt, M. Stolte, F. Würthner, *Chem. Eur. J.* **2021**, *27*, 11997–12006.
[42] J. Li, P. Li, M. Fan, X. Zheng, J. Guan, M. Yin, *Angew. Chem. Int. Ed.* **2022**, *61*, e202202532.

[43] Deposition Numbers 2221170 and 2221169 contain the supplementary crystallographic data for this paper. These data are provided free of charge by the joint Cambridge Crystallographic Data Centre and Fachinformationszentrum Karlsruhe Access Structures service.
[44] C. Goedicke, H. Stegemeyer, *Tetrahedron Lett.* **1970**, *11*, 937–940.
[45] A. L. Spek, *Acta Crystallogr. Sect. A* **1990**, *46*, C43.
[46] T. Kaehler, A. John, T. Jin, M. Bolte, H.-W. Lerner, M. Wagner, *Eur. J. Org. Chem.* **2020**, 5847–5851.
[47] M. Rickhaus, L. Jundt, M. Mayor, *Chimia* **2016**, *70*, 192.
[48] P. Ravat, *Chem. Eur. J.* **2021**, *27*, 3957–3967.
[49] T. Hartung, R. Machleid, M. Simon, C. Golz, M. Alcarazo, *Angew. Chem. Int. Ed.* **2020**, *59*, 5660–5664.
[50] N. Ousaka, S. Yamamoto, H. Iida, T. Iwata, S. Ito, Y. Hijikata, S. Irle, E. Yashima, *Nat. Commun.* **2019**, *10*, 1457.
[51] A. D. Becke, *J. Chem. Phys.* **1993**, *98*, 5648–5652.
[52] C. Lee, W. Yang, R. G. Parr, *Phys. Rev. B* **1988**, *37*, 785–789.
[53] S. H. Vosko, L. Wilk, M. Nusair, *Can. J. Phys.* **1980**, *58*, 1200–1211.
[54] P. J. Stephens, F. J. Devlin, C. F. Chabalowski, M. J. Frisch, *J. Phys. Chem.* **1994**, *98*, 11623–11627.
[55] S. Grimme, J. Antony, S. Ehrlich, H. Krieg, *J. Chem. Phys.* **2010**, *132*, 154104.
[56] S. Grimme, S. Ehrlich, L. Goerigk, *J. Comput. Chem.* **2011**, *32*, 1456–1465.
[57] F. Weigend, R. Ahlrichs, *Phys. Chem. Chem. Phys.* **2005**, *7*, 3297–3305.
[58] A. V. Marenich, C. J. Cramer, D. G. Truhlar, *J. Phys. Chem. B* **2009**, *113*, 6378–6396.
[59] Y. Zhao, D. G. Truhlar, *J. Phys. Chem. A* **2005**, *109*, 5656–5667.
[60] L. Goerigk, R. Sharma, *Can. J. Chem.* **2016**, *94*, 1133–1143.
[61] P. R. Horn, Y. Mao, M. Head-Gordon, *Phys. Chem. Chem. Phys.* **2016**, *18*, 23067–23079.
[62] N. Mardirossian, M. Head-Gordon, *J. Chem. Phys.* **2016**, *144*, 214110.
[63] S. Grimme, *Angew. Chem. Int. Ed.* **2008**, *47*, 3430–3434.
[64] S. Grimme, C. Mück-Lichtenfeld, J. Antony, *J. Phys. Chem. C* **2007**, *111*, 11199–11207.
[65] Á. J. Jiménez, M.-J. Lin, C. Burschka, J. Becker, V. Settels, B. Engels, F. Würthner, *Chem. Sci.* **2014**, *5*, 608–619.
[66] A. Nowak-Król, M. I. S. Röhr, D. Schmidt, F. Würthner, *Angew. Chem. Int. Ed.* **2017**, *56*, 11774–11778.

Manuscript received: January 26, 2023
Accepted manuscript online: March 13, 2023
Version of record online: April 4, 2023